Large Signal Impedance of Resonant Tunneling Diodes

J. F. Lampin*,O. Vanbésien*, O. Tanguy* and D. Lippens*

Abstract: The large signal impedance of resonant tunneling diodes has been evaluated using reflection coefficient measurements and power measurements for self-oscillating devices. To this aim, small area devices were fabricated with necessary coplanar lines for microwave wafer probing in a low parasitic planar technology. For large applied or self-sustained rf voltages, marked differences between the slope of the I(V) curve at the bias point (small signal conditions) and the large signal conductance have been found. These measurements have been interpreted satisfactorily on the basis of self-consistent treatment of the power delivered (generated) to (by) the diodes and of Fourier transforms of the current components.

Introduction: In recent years, there has been an intensive effort in the development of high frequency nonlinear applications on the basis of double barrier Resonant Tunneling Diodes (RTD's) used as oscillators, harmonics multipliers, detectors and mixers. Beyond the benefit that the resonant tunnelling effect can be very fast, interest in these devices is motivated by pronounced room temperature Negative Differential Conductance effect(NDC).While the small signal impedance is now well understood with frequency measurements at microwave and millimeter wavelengths, relatively little attention has been paid to impedance under large signal conditions. Recently O. Boric-Lubecke et al.[1] have analyzed large signal negative conductance for predicting the output power and conversion efficiency of a quantum well oscillator. Other results were published by S.M. Nilsen and L. Lundgren[2] for describing the maximum available output versus oscillation frequency. Since our first measurements we carried out in negative differential resistance by cooling a GaAs/AlGaAs sample down to 77K[3], we have reported extensive measurements at room temperature[4] and up to 40 GHz recently[5]. In this work we take advantage of this know-how to study in what extent the large signal impedance can be measured directly and related to the physical device.

Measurement conditions: Figure 1 shows the essential features to understand the conditions for successfully measuring the large signal impedance. In brief, we can distinguish three parts in the I-V curve which correspond to various conduction regimes. The first one, close to equilibrium, is achieved when the tunneling current components between emitter and collector and reciprocally are unbalanced. It can be shown that the current grows exponentially against voltage as demonstrated by measuring the first and the second derivatives of current with to respect V. The second part corresponds to the NDC regime when the resonant enhancement of the overall transmission is lost. The subsequent drop in the current values depends on device structure and notably on spacer layers which acts as "lever arms" and thus amplify the voltage values. Nevertheless as a general rule, an abrupt transition can be noticed for bias close to Vp whereas , in the vicinity of the valley voltage Vv the change in current is more gradual. In passing, let us note that, in this last range of the characteristics, accurate measurements of the small signal impedance can be made provided the stability criteria are satisfied. In the third part, the current exhibits again an exponential dependence versus voltage. This was recently demonstrated and used to quickly determine the series resistance[6].

The voltages involved in the various processes are typically of a few hundreds millivolts. This means that the large signal admittance (impedance) can be measured simply if we succeed in optimizing the power transfers between the device under test and the analysis tool. For a given heterostructure and hence current density and voltage, a common method is

to vary the device area in the range of a few square microns so that the conductance level fits the source. In the following, we will see that jointly the imaginary part vanishes.

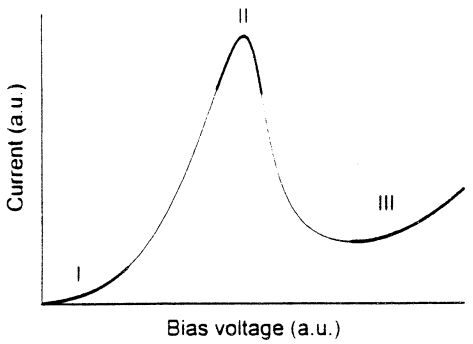

Fig. 1 Schematic of RTD's I-V characteristics

GaAs	3 10^{18} cm^{-3}	500 nm
GaAs	1 10^{17} cm^{-3}	10 nm
GaAs	Undoped (UD)	5 nm
$In_{0.1}Ga_{0.9}As$	UD	5 nm
GaAs	UD	0.5 nm
AlAs	UD	1.7 nm
GaAs	UD	0.5 nm
$In_{0.1}Ga_{0.9}As$	UD	4 nm
GaAs	UD	0.5 nm
AlAs	UD	1.7 nm
GaAs	UD	0.5 nm
$In_{0.1}Ga_{0.9}As$	UD	5 nm
GaAs	UD	5 nm
GaAs	1 10^{17} cm^{-3}	10 nm
GaAs	3 10^{18} cm^{-3}	500 nm
SI Substrate		

Fig. 2 Growth sequence

Fabrication: Resonant tunneling diodes were fabricated from pseudomorphic epitaxies in the InGaAs/AlAs/GaAs material system. The fact to introduce InGaAs strained layers permits one to decrease the peak voltage while maintaining spacer layers which guarantee epitaxial quality. Fig. 2 describes the various layers of growth sequence starting from a semi-insulating substrate. Barriers with thickness of 1.4nm were here chosen in order to achieve relatively high current density , a key feature for a high frequency operation. In return, we will see that the diodes cannot be stabilized over the overall NDC bias range. These considerations are the primary motivations for developing a two-step mesa technology using air-bridge techniques which permit to integrate small area devices and to maintain the parasitic element at an extremely low level.

Figure 3 gives a scanning electron micrograph of an air-bridged representative device. For the present case the lateral dimensions were about 2μm by 10μm. Detailed of technological processes can be found elsewhere[7]. In brief, top contacts were formed by defining AuGeNi ohmic contacts by lift off techniques and by chemically etching down to the n+ buffer layer to implement the side contacts. A secondary mesa isolation was then formed leaving the semi-insulating substrate exposed where coplanar transmission lines were deposited. Top contacts and central lines were interconnected by means of air-bridges formed by evaporation or electroplating. Figure 4 gives the I-V curve of a representative device in forward and reverse bias directions measured at room temperature with dc probes and a curve tracer. The devices exhibit a high degree of symmetry in the I-V which is a good indicator of epitaxial quality. As expected, instabilities in NDC bias distord the characteristics which otherwise verify the general considerations aforementioned. Peak current densities are typically 50kAcm^{-2}. Peak-to-valley current ratios vary between 5:1 to 7:1. The peak voltage is 600mV for a voltage excursion for NDC effects of about 400mV.

Fig. 3 SEM of an air-bridged device

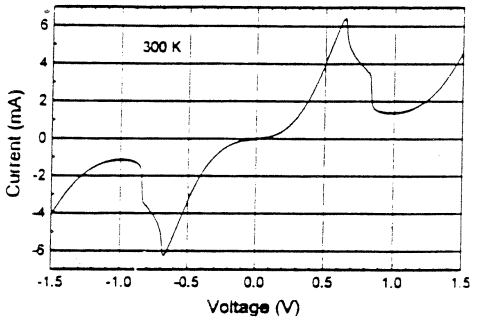

Fig. 4 Typical I(V) at 300K

Small signal impedance: At this stage, a first idea of the voltage dependence conductance can be achieved by dc characterizing the devices by means of low inductance microwave probes and by taking the derivative of the I-V characteristics. A typical plot of the small signal conductance corresponding to the slope of the I-V curve at each bias point is given in Figure 5 over the whole range of interest. Close to equilibrium, conductance varies quasi-exponentially. In the NDC region, spikes in the conductance are apparent due to the well-known shoulder-like I-V variations resulting from self-biasing effects. Close to Vv and hence at high impedance level , devices are unconditionally stable. In that case, impedance measurements can be conducted and the device reflection coefficient exceeds unity . This voltage range over which the characterization in NDC makes sense is however very narrow. This implies that , under large signal conditions, the rf swing superimposed on the bias voltage exceeds very rapidly this voltage range for stability. One way to overcome this drawback is to further decrease the device area. This requires to use more advanced technological resources notably direct writing of anode (cathode) patterns by electron beam lithography at submicron scale.

Turning now to the voltage dependence of G close to V=0V we obtained the results depicted in Figure 6. Pronounced variations can be evidenced over a voltage range of a few tens of millivolts It is worth mentioning the role played by the series resistance due to contact and epitaxial layers . Indeed, for high current drivability samples the rise in current versus voltage can be affected by the voltage drop across the access resistance. As a consequence, the intrinsic nonlinearity of the tunneling process can be seriously attenuated and even completely vanishes in case of poor contact resistivity.

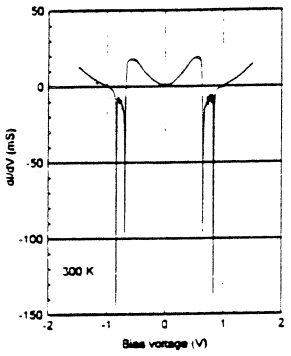

Fig. 5 Conductance versus voltage (Area=20μm^2)

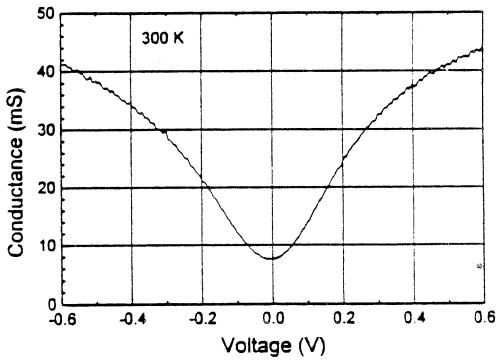

Fig. 6 G(V) in PDC region (Area=100μm^2)

The frequency dependence of the small signal impedance, used for comparison in the following, is exemplified in Figure 7. Here , measurements were made by means of rf probes up from 0. 5 to 40 GHz , when the device is biased in NDC region. The figure gives a Smith chart plot of S11 scattering parameter at diode terminals. The magnitude of outer circle is 2.5. At 40 GHz, impedance Z is -30-j52 Ω. No oscillating behavior was detected in this case . At higher frequencies the negative resistance rolls off and goes positive by intersecting the inner circle of unitary magnitude. Such a characterization over a broad frequency band can also be used to accurately derive an equivalent circuit for the dipole which is of importance for evaluating the ratio between available and delivered powers and subsequently the rf voltage swing across the diode. To this aim we used the lumped-element circuit, reported in figure 8, very similar to that of the Esaki tunnel diode. It consists of a single capacitor Cd with a parallel negative resistance Rd. These intrinsic elements are completed by the parasitic capacitance Cp and inductance Lp due to interconnects and Rs the overall series resistance. "A priori", one should expect also a variation of the capacitance against voltage. Indeed, the capacitance of the

diode measured at lower frequency was found almost constant because the diode is rapidly under punch-through conditions. Here again attention has to be paid to the series resistance which can lead to an apparent variation of Cd versus V when the relation Rd/Rs >>1 is not satisfied. In practice, the determination of the lumped elements can be made very accurately by measuring samples with different areas, shifting by this way the resonance frequencies introduced by Lp and by varying the bias conditions. The parasitic capacitance contribution was determined with open circuited devices. Finally, we found for the S11 plot of Figure 7 Rd=-180Ω, Cd=37fF, Rs=9Ω, Lp=60pH, Cp=13fF values which gives the best fit with experimental data.

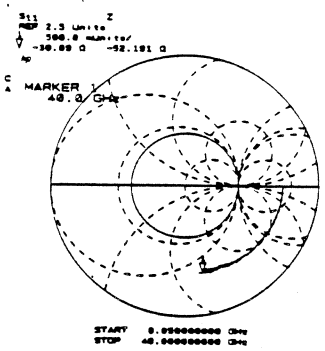

Fig. 7 Frequency dependence of S11
Small signal conditions

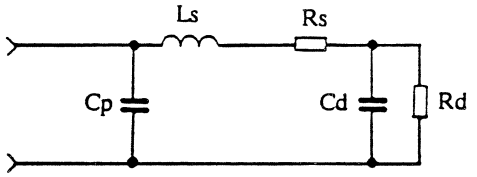

Fig. 8 Equivalent circuit

Large signal conditions: Increasing the power delivered by the generator of network analyzer(HP 8510) leads to drastic changes in the measured values of impedance. Figure 9 gives typical variations we obtained up to 26GHz when the device is unbiased for two values of attenuation and hence of incident power P_{in}. Here device area is 100μm^2. An attenuation value of 20dB corresponds to a measure under small signal conditions because decreasing further P_{in} does not affect the results. At low frequencies the differences are particularly important whereas at high frequencies they are progressively attenuated. This can be explained by the fact that in the present case the power delivered by the generator is not constant. This can be checked in Figure 10 which gives the incident power at port 1 measured with a bolometer. Measurements at constant power can be conducted however by narrowing the analysis window. Therefore, the highest incident power which was possible to apply was 800μW without distortion in the detection. This level was kept constant up to 6GHz. The results achieved for this case are plotted in Figure 11 along the variations of the small signal impedance. With an increase of the power absorbed at diode terminals the real part becomes progressively insensitive to frequency and the imaginary part tends to vanish. These results have been obtained for a 20 μm^2 area sample.

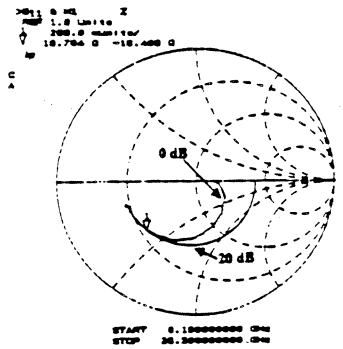

Fig 9 S_{11} versus frequency for two attenuations

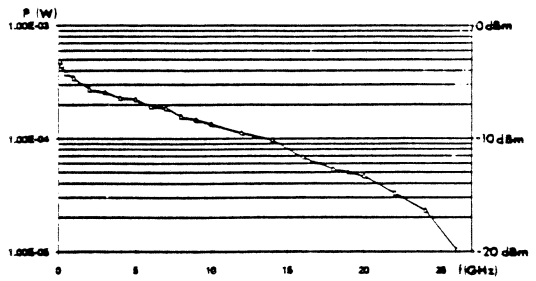

Fig. 10 P_{in} versus frequency

Further insight into this natural matching between source and device can be obtained by plotting the frequency dependence of the real and imaginary part of impedance respectively taking Rd as a parameter. The results of these calculations by varying Rd between 10 and 100Ω with a step of 10 Ω are reported in Figure 12 for the following circuit elements Cd= 42fF, Ls=65pH and Cp=15fF. For Rd = 20Ω one can note that Re(Z) in the input plane is very close to 50Ω between 0 and 50 GHz and Im(Z) practically vanishes.

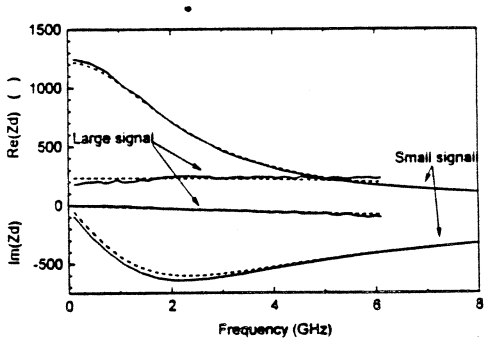

Fig 11 Comparison of large and small signal impedances

This effective matching can be experimentally verified notably when the device is biased at voltages close to Vp. At this bias point , for a 20μm^2 device the diode resistance is typically 20Ω as it was required previously. The variations of Z as a function of frequency we measured for a 20dB attenuation are displayed in Figure 13. At the marker frequency Re(z) is 51. 3 Ω and Im(Z) is -2Ω. In this Figure, it can also be seen that large signal measurements (0dB) lose their meaning (presence of strong instabilities) because the large rf signal reaches the zone of high NDC.

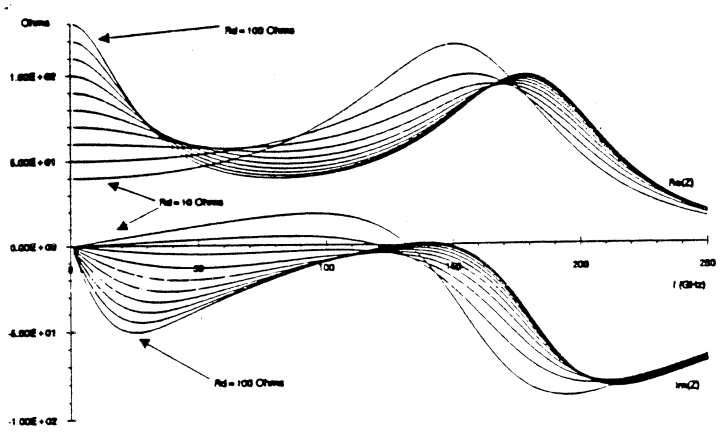

Fig. 12 Z(f) calculated for various resistance values

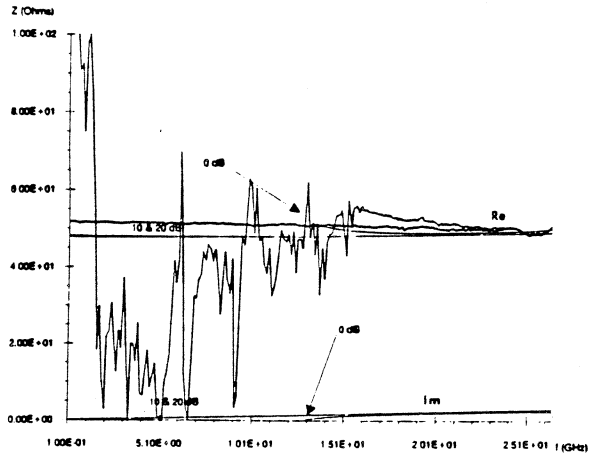

Fig. 13 Variations of impedance for bias close to V_{peak} under small and large signal conditions

In order to analyze the experiment reported above, a simulation program was written to calculate the large signal impedance. For sake of simplicity, only the fundamental frequency component of the rf voltage was assumed while the current harmonics were taken into account. For calculating the voltage swing across the resistance, we have self consistently evaluated the power transfer between the source and the resonant tunneling diode. Starting from small signal impedance values the conductance level was iteratively updated as a function of the transfer efficiency. For this calculation of G, the current waveform I(t) is derived from the dc I-V curve . From a Fourier series expansion of I(t), the large signal conductance is then found as G=I1/Vrf where I1 is the current amplitude at the fundamental frequency. The procedure is repeated until convergence on G is obtained Using this procedure, agreement between measured and calculated values is excellent as noted in figure 11 which gives a comparison between theory and experiment.

The large signal conductance cannot be measured directly when the devices exhibit strong NDC effect as noted before However it is possible to extract this information when the diodes are used as oscillators. To this end devices were mounted in a rf test fixture in order to achieve a free running sinusoidal oscillation. From a $9\mu m^2$ area device, oscillations in the frequency range 18-23GHz were thus obtained. In figure 14 a typical oscillation spectrum is displayed at a frequency of 19.7GHz. The highest output power we achieved was $83\mu W$. For the derivation of G the measured part of the I-V curve was fitted in the NDC region by a $\tan^{-1}$ function which is connected to the stable region of the characteristic. In Figure 15 the validity of the fit can be verified. On the basis of this approximation the rf voltage dependence of G can be calculated at various bias voltages and notably at the bias for oscillation. For the later the large signal G exhibits a maximum at V_{rf}=200mV.

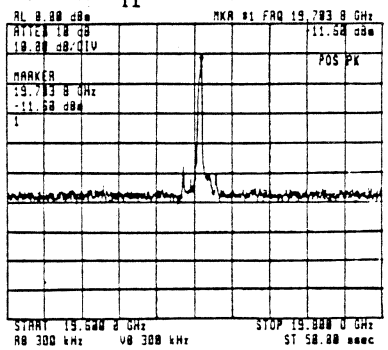

Fig. 14 Oscillation spectrum for the device mounted in a rf test-fixture

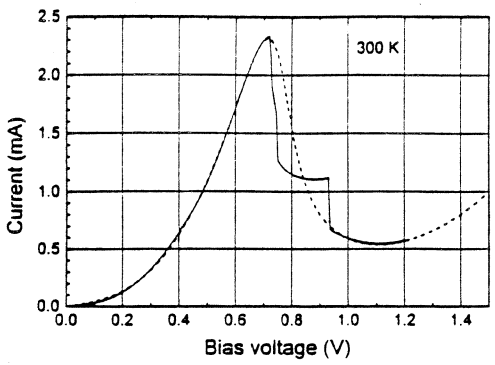

Fig. 15 Measured and fitted I-V curves

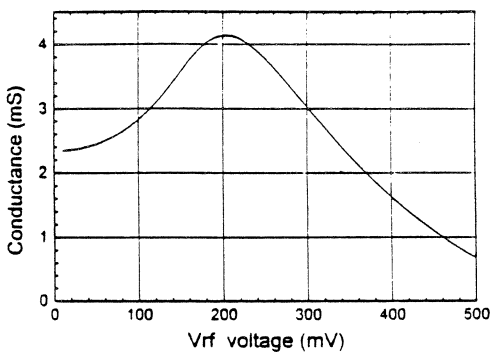

Fig. 16 Calculated large signal conductance

Conclusion: The impedance of Resonant Tunneling diodes have been characterized under small and large signal conditions by direct measurement of reflection coefficients using a network analyzer and by analysis of the output power for devices used as oscillators. Using a Fourier transform of I(t), after evaluation of the rf voltage at diode terminals the large signal conductance have been calculated and compared satisfactorily with experiment.

This work was supported by the D.R.E.T.(Contract 91.099)

Acknowledgements: We would like acknowledge the technical assistance of E. Delos

---

*J.F. Lampin, O. Vanbésien, O. Tanguy and D. Lippens are with
Institut d'Electronique et de Microélectronique du Nord
Avenue Poincaré, BP 69, 59652 Villeneuve d'Ascq, France

[1]O. Boric-Lubecke, et al.,Conference proceedings EuMC,Sept 1993, pp817-818

[2]S. M. Nilsen, et al.,Microwave and Optical Technology Letters,Vol. 6,No.11,Sept.1993, pp621-623

[3]D. Lippens, et al., Electronics Letters, Vol. 24, No. 18, Sept. 1988, pp1180-1181

[4]O. Vanbésien, et al., Microwave and Optical Technology Letters, Vol. 5, No. 8, July 1992, pp351-354

[5]P. Mounaix, et al., Electronics Letters, Vol. 27, No. 15, July 1991, pp1358-1359

[6]M. J. Deen, Electronics Letters, Vol. 28, No 13, June 1992, pp1195-1197

[7]E. Lheurette, et al., Electronics Letters, Vol. 28, No. 10, May 1992, pp937-938